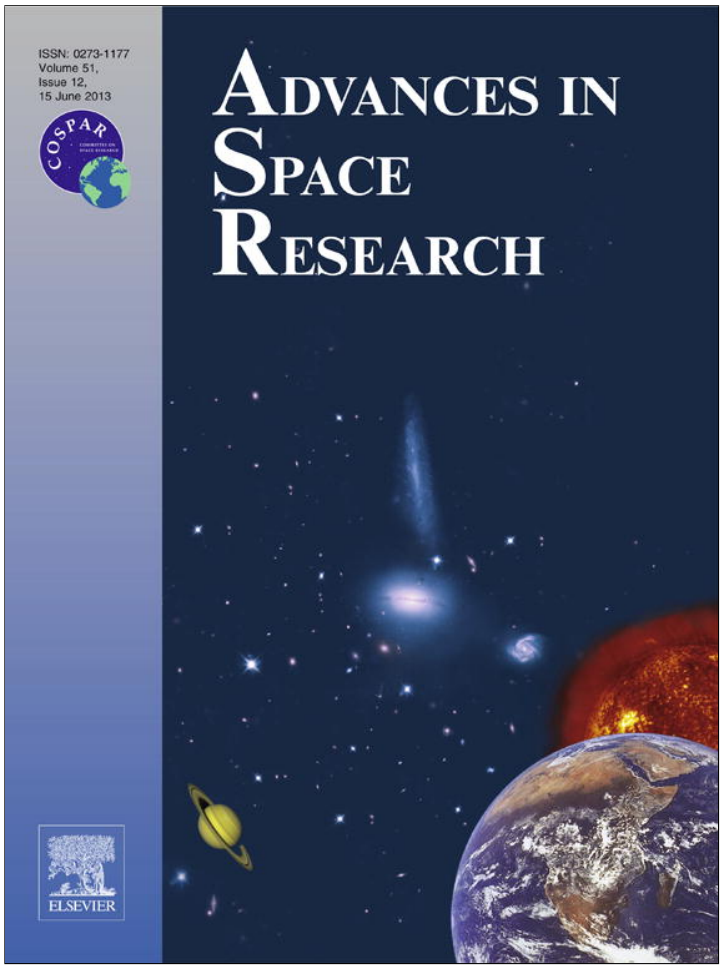

Available online at www.sciencedirect.com

SciVerse ScienceDirect

Advances in Space Research 51 (2013) 2195–2206

ADVANCES IN SPACE RESEARCH (a COSPAR publication)

www.elsevier.com/locate/asr

Local orbital debris flux study in the geostationary ring

Paul V. Anderson *[,1], Hanspeter Schaub [2]

University of Colorado, Boulder, CO 80309, United States

Received 18 September 2012; received in revised form 11 January 2013; accepted 14 January 2013
Available online 30 January 2013

Abstract

A local orbital debris flux analysis is performed in the geostationary (GEO) ring to investigate how frequently near-miss events occur for each longitude slot in the GEO ring. The current resident space object (RSO) environment at GEO is evaluated, and publicly-available two-line element (TLE) data are utilized in tandem with a geostationary torus configuration to simulate near-miss events incurred by the trackable RSO population at GEO. Methodology for determining near-miss events with this formulation is introduced, and the results of the analysis for a one-year time frame are provided to illustrate the need for active GEO remediation.

Keywords: Geosynchronous orbit; Orbital debris; Debris flux

1. Introduction

The geostationary (GEO) ring is a precious commodity of the terrestrial satellite industry that has become contaminated with an alarming number of orbital debris objects (Jehn et al., 2005; Johnson, 1999; Wegener et al., 2004; Chrystal et al., 2011). Defunct, decommissioned satellites, upper launch vehicle stages, and fragmentation particulates continuously threaten satellites operating in this regime. As the lack of atmospheric drag effects at the GEO altitude renders the lifetimes of these debris objects infinitely long (Yasaka et al., 1999; Yasaka, 2002; Klinkrad, 2006; Jehn and Hernandez, 2001), conjunction and mitigation assessment must be performed to safeguard functional GEO satellites from colliding with the surrounding debris field. GEO satellites must maintain a specific longitude, and thus cannot simply phase shift to evade debris. Analysis of the *macroscopic* behavior of the geostationary debris field is therefore required to describe debris fluxes through GEO longitude slots, to forecast how often operational satellites in these regions must potentially perform maneuvers to mitigate conjunction scenarios. Instead of presenting highly-accurate analysis required for risk assessment and mitigation (Alfriend et al., 1999; Klinkrad et al., 2005), this study fills a void in the literature by illustrating gross behavior of the resident space object (RSO) population at GEO, to discern which *local* regions of the GEO ring are most susceptible to rising debris fluxes at different times. This information must be accounted for by owners and operators when preparing to occupy a GEO longitude slot, as it is an indicator of how much maneuvering fuel must be included on-board prior to launch and slot insertion.

Existing debris analysis and evolution software (Liou et al., 2004; Bendisch et al., 2004; Lewis et al., 2001) employ inertial cell definitions to track debris cell passage events (CPE) arising from the intersections of osculating RSO orbits with the cells of interest during long-term propagation; using various probability models, the associated spatial density and flux contributions for each CPE may thereafter be computed and implemented for conjunction risk assessment. For the GEO regime, these analysis tools often average over cell right ascension, providing debris

* Corresponding author.
E-mail addresses: paul.anderson@colorado.edu (P.V. Anderson), hanspeter.schaub@colorado.edu (H. Schaub).
[1] Department of Aerospace Engineering Sciences, 429 UCB, Boulder, CO 80309, United States.
[2] H. Joseph Smead Fellow, Associate Chair of Graduate Affairs, Department of Aerospace Engineering Sciences, 429 UCB, Boulder, CO 80309, United States.

0273-1177/$36.00
http://dx.doi.org/10.1016/j.asr.2013.01.019

fluxes as a function of altitude and declination (Klinkrad, 2006). Furthermore, utilizing inertially-fixed cell definitions only, flux contributions to particular GEO longitude slots at arbitrary epoch times cannot be determined. Therefore, though *average* flux conditions at GEO may be estimated with such tools, *local* intersection events for certain longitude slots are not accessible. The latter is of interest to space operators concerned with the debris conditions near a functioning satellite. This study implements a toroidal cell configuration at the GEO altitude to evaluate the impact of the current RSO population on the longitude slots at GEO, by performing a near-miss analysis that attempts to quantify the frequency at which uncontrolled RSOs pass within a given distance of a particular GEO slot. Thereby, in order to enhance intuition, an integer number of near-misses is used here as the alternative to typical density and flux metrics (Klinkrad, 2006).

Such a near-miss CPE study is critical, as it provides a metric as to how frequently a GEO satellite operator will have to track nearby debris motion, and potentially execute avoidance maneuvers. The latter is of particular importance, as avoidance maneuvers (though generally not mission-interrupting for GEO satellites) can temporarily force a satellite out of its specified longitude slot, which may potentially pose problems for the mission at hand, and be difficult to manage if neighboring satellites are collocated in the same station-keeping slot. Currently, the GEO RSO population is sparse enough such that a simple time-shift of a scheduled maintenance maneuver is sufficient for evading debris – in these situations, no additional propellant is expended beyond that allocated for routine station-keeping. However, as the GEO debris population continues to increase unchecked, the amount of propellant required to remain at a specified longitude slot while simultaneously mitigating conjunctions will begin increasing as well. The focus of this study is to propose a near-miss metric and illustrate current conditions at GEO. This metric can then be harnessed in future efforts as the impact of continued, uninhibited debris generation—or conversely, active removal to disposal orbits—is investigated.

Although current probability of collision at GEO has been assessed as relatively low as compared to that in the low-Earth orbit (LEO) regime (Chrystal et al., 2011; Liou, 2011), collision risk will grow if mitigation and remediation measures are not globally adopted and implemented. This study illustrates the current status of near-miss events at GEO, given the trackable RSO population in this regime, to serve as a benchmark for continuing studies that will demonstrate the future severity of this environment under projected growth without remediation. The total insurance value of on-orbit assets in the GEO regime is estimated at USD 20 billion (Chrystal et al., 2011) – debris analysis studies therefore have strong implications for satellite owners/operators that desire to preserve continuing usefulness of this resource, by forecasting debris field evolution and providing recommendations for mitigation in this regime.

2. Current RSO population at GEO

The status of the RSO population currently in the geosynchronous regime is presented as a precursor to the flux study performed in this research. Section 2.1 describes the orbit classification system implemented and highlights the tracking data source used; Section 2.2 briefly illustrates the distribution of this population.

2.1. Classification of geosynchronous objects

The RSO population in the geosynchronous arena is classified with a taxonomy used by the European Space Agency's DISCOS Database (Database and Information System Characterising Objects in Space) and updated by the European Space Operations Centre (ESOC) Space Debris Office (Flohrer, 2012). For geosynchronous RSOs, seven orbit categories are established to classify the type of geosynchronous orbits traversed by these objects; Table 1 provides a description of this classification system. Geosynchronous objects are selected according to (Flohrer, 2012):

- Eccentricity smaller than 0.2 ($e < 0.2$);
- Inclination smaller than 70° ($i < 70°$);
- Mean motion between 0.9 and 1.1 revs per sidereal day ($0.9 < n < 1.1$).

Orbit data for the trackable GEO RSO population are obtained from publicly-available two-line element (TLE) sets provided by U.S. Strategic Command (USSTRATCOM).[3] For this debris flux study, a reference TLE set obtained on 02/15/12 is employed; the class distribution for the 1070 objects extracted from this set is illustrated in Fig. 1. Note that while approximately one-third of this RSO population is under control, half of the RSO population is hazardously drifting above, below, or through the GEO altitude. Fig. 2 quantifies the influence of orbit eccentricity on penetration of the "protected" GEO zone, defined as the region located within ±200 km and ±15° latitude of the GEO ring (IADC/WG4, 2007; NASA, 2009). Although the semi-major axis of a given RSO may deviate from the geostationary radius, high eccentricity may "slingshot" such an object through this protected zone towards radius of perigee or apogee.

TLE data are provided as doubly-averaged Keplerian elements (Klinkrad, 2006) with mean motion instead of semi-major axis, transformed into Cartesian states in the true equator, mean equinox (TEME) frame (Vallado, 2007) with SGP-4 theory (Hoots et al., 1980) for this flux study.[4] The TLE data provide additional information on

[3] Publicly-available TLE data sets (updated twice daily) are available for bulk download from: <https://www.space-track.org/>.

[4] ANSI-C implementation of merged SGP-4/SDP-4 theory for TLE processing is available from: <http://www.sat.dundee.ac.uk/psc/sgp4.html>. (Vallado et al., 2006).

Table 1
Orbit classifications for geosynchronous objects used in GEO debris flux study.

Class	Type	Description
C1	Controlled	Longitude/inclination control (E–W/N–S control)
C2	Controlled	Longitude control only (E–W control only)
D	Drifting	Drift above/below/through protected GEO zone
L1	Librating	Libration about Eastern stable point ($\lambda = 75°$E)
L2	Librating	Libration about Western stable point ($\lambda = 105°$W)
L3	Librating	Libration about Eastern/Western stable points
IN	Indeterminate	Unknown status (e.g., recent TLE not available)

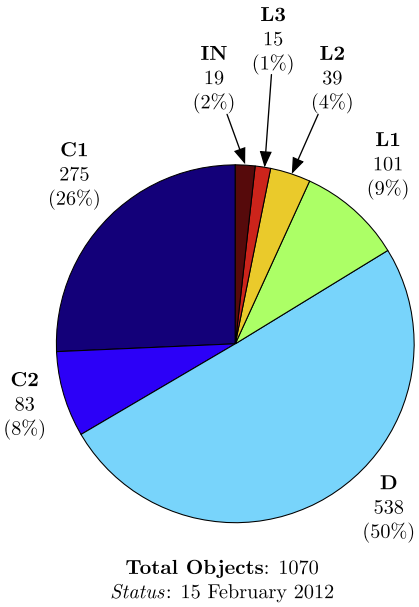

Fig. 1. Distribution of GEO RSO population.

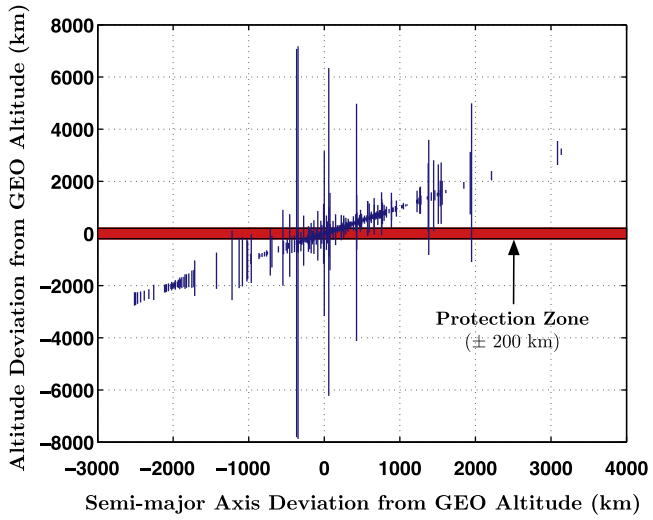

Fig. 2. Distribution of drifting population (each line represents one RSO).

the reference TLE epoch and international designation code (COSPAR designation[5]) for each of these tracked RSOs. Note that because of the limited accuracy of the TLE sets, these data are *not meant for high-precision analyses*; as the purpose of this study is to characterize near-miss events occurring on a macroscopic scale, the accuracy of these data is appropriate for this study. For higher-accuracy studies, multiple TLE sets may be implemented as pseudo-observations in an initial orbit determination routine, to "best" recover osculating orbits suitable for propagation with a high-fidelity force model (Klinkrad, 2006).[6] Furthermore, only objects larger than one meter are routinely tracked at the GEO altitude (Flohrer, 2012) – thus, only unclassified RSOs at least of this size are considered here.[7]

Additionally, note that although 1070 objects from the 02/15/12 TLE set satisfied the above criteria for a GEO designation, 238 more objects without up-to-date TLE data are known to reside within this regime (Flohrer, 2012). Therefore, there exist (at least) a total of 1308 RSOs near the geosynchronous altitude. In Flohrer (2012), data for 164 of the 238 objects for which current tracking data are not available were provided by the Keldysh Institute for Applied Mathematics (KIAM); these RSOs are not accounted for here. Since this study only incorporates the trackable, catalogued, and unclassified GEO RSOs with up-to-date TLE data, the findings of this study serve to illustrate the conservative lower bound of the true debris situation in the GEO regime.

2.2. Distribution of geosynchronous objects

Implementing the 02/15/12 reference TLE considered for this study, the projected RSO population distribution as of 03/01/12 (the start date of the near-miss CPE analysis) is evaluated using the orbit propagator detailed in Section 3.3. A snapshot of the GEO RSO population on this date is provided in Fig. 3(a); the longitude distribution of these 1070 RSOs is illustrated in Fig. 3(b). Note the high concentration of librating objects in the vicinity of the

[5] During processing of a TLE data set, COSPAR identifiers are checked against Flohrer, 2012 (COGO-14) for class assignment.

[6] Though SGP-4 implementations may be used for directly propagating TLE sets, SGP-4 theory is employed here *only* to recover initial conditions, which are subsequently propagated under software developed by the authors (see Section 3.3). The models incorporated in this tool are readily changeable, and facilitate high-performance computing capabilities.

[7] USSTRATCOM collects tracking data for GEO with the GEODSS (Ground-Based Electro-Optical Deep-Space Surveillance) and MOTIF (Maui Optical Tracking and Identification Facility) installations, part of the Space Surveillance Network (SSN) (Klinkrad, 2006).

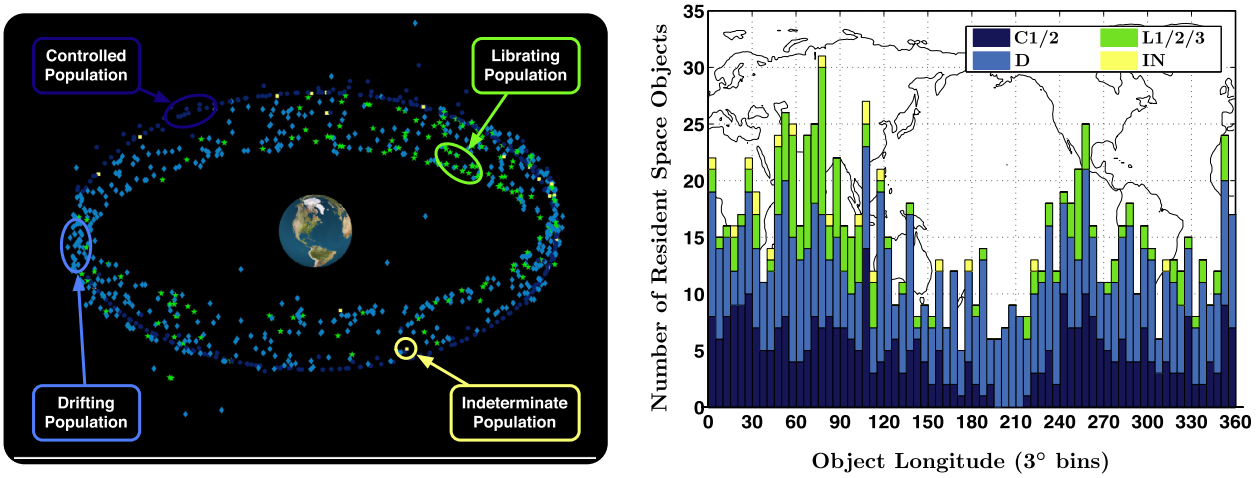

(a) Visualization of GEO RSO population. (b) Longitude distribution of GEO RSOs.

Fig. 3. Distribution of GEO RSO population on 03/01/12 using 02/15/12 TLE set.

Eastern and Western stable points. Drifting objects, though distributed approximately uniformly around the GEO regime, pose less of a hazard to the longitude slots over the Pacific Ocean, in which controlled (C1/C2) on-orbit assets are at a minimum. Again, instead of stipulating averaged spatial densities at GEO, this study evaluates *localized* densities by simulating near-miss events for each longitude slot in the GEO ring.

3. Local debris flux study at GEO

A debris flux study in the geostationary ring is performed to quantify the number of near-misses occurring in a one-year time frame for every longitude slot at GEO – therefore, the results of this study seek to quantify *how often* operational satellites residing in this regime potentially need to maneuver to avoid impending conjunction with a nearby RSO, given the current, trackable geosynchronous debris population. Section 3.1 presents a torus concept employed for performing this study, and Section 3.2 mathematically formulates near-miss intersections. Section 3.3 describes the force model implemented in propagation, and Section 3.4 presents the results of the study for a one-year period to forecast local "debris weather" in the GEO ring.

3.1. Geostationary torus concept

Near-miss events for the GEO longitude slots are determined by formulating a GEO-encompassing torus of major radius $r_{GEO} = 42164$ km and minor radius $\tilde{r}$, as depicted in Fig. 4. Torus cells implemented for tracking the near-miss events are constructed by partitioning this torus with longitude increments of $\Delta\lambda$. For this study, $\Delta\lambda = 1^\circ$ is used, and minor radii of $\tilde{r} = 50$ km, 100 km, 300 km and 700 km are simulated to evaluate the frequency of near-miss CPE occurring from distances representative of a 1° longitude

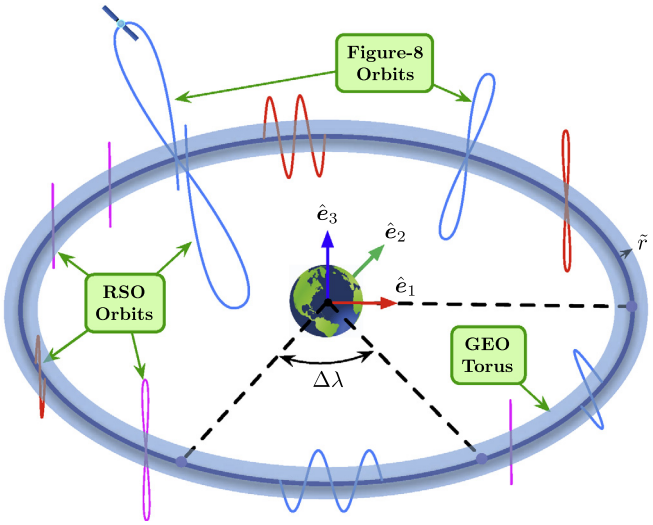

Fig. 4. Geostationary torus concept implemented in near-miss study.

slot at GEO (~700 km) to distances at which precise conjunction assessment and analysis roughly could be considered (~50 km). Furthermore, this torus formulation is a natural choice for evaluating CPE for the non-inertial GEO longitude slots – the torus geometry is invariant as seen by both the inertial frame (i.e., J2000) and the Earth-centered, Earth-fixed frame (in which these longitude slots are fixed). Thus, coordinate transformations are not required in this formulation.

Furthermore, Fig. 4 also illustrates several examples of the complex relative RSO motion experienced by operational GEO satellites in the course of one day. As natural perturbations (especially the lunar gravity influence) increase the inclination of near-synchronous RSOs, but do not appreciably alter the orbital radius, these objects trace north-south routes that interact with the GEO ring at ascending and descending nodes (Yasaka et al., 1999). Geosynchronous, inclined RSOs exhibit a north–south

motion that appears as a straight line from an observer fixed upon the Earth. The near-synchronous objects that deviate from the GEO altitude additionally exhibit an east/west drift that superimposes upon this north–south motion to establish the sinusoidal and "figure-8" trajectories illustrated in Fig. 4 – these relative orbits precess eastward for RSOs below the GEO altitude, and regress westward for RSOs above the GEO altitude. In each of these cases, luni-solar gravitation induces an increase in inclination of approximately 0.8° per year; this effect is periodic, however, and inclination begins to regress to 0° after achieving 15°, with a period of approximately 26 years (Yasaka et al., 1999; Chao, 2005).

3.2. Formulation of cell passage events

Near-miss CPE are detected during forward propagation of a particular near-synchronous RSO by checking for transversal of the GEO torus boundary at each time step of numerical integration (the integration routine used for this research is highlighted below within Section 3.3). Mathematically, a near-miss event occurs if

$$\left(r_{\text{GEO}} - \sqrt{r_X^2 + r_Y^2}\right)^2 + r_Z^2 - \tilde{r}^2 < 0 \tag{1}$$

is satisfied, wherein $(r_X, r_Y, r_Z)^T$ is the RSO position vector expressed in the inertial reference frame, $r_{\text{GEO}} = 42164$ km is the major torus radius, and $\tilde{r}$ is the specified minor radius. The longitude of intersection λ_{CPE} is thereafter determined with

$$\lambda_{\text{CPE}} = \arctan\left(\frac{r_Y}{r_X}\right) - \alpha_G \tag{2}$$

wherein α_G is the right ascension of Greenwich, determined with the following methodology (Curtis, 2005):

$$J_0 = 367t_y - \text{floor}\left(\frac{7}{4}\left[t_y + \text{floor}\left(\frac{t_m + 9}{12}\right)\right]\right) + \text{floor}\left(\frac{275t_m}{9}\right) + t_d + 1721013.5 \tag{3a}$$

$$T_0 = \frac{J_0 - 2451545}{36525} \tag{3b}$$

$$\alpha_{G0} = 100.4606184 + 36000.77004T_0 + 0.000387933T_0^2 - 2.583(10^{-8})T_0^3(\text{deg}) \tag{3c}$$

$$\alpha_G = \alpha_{G0} + 360.98564724\left(\frac{t_h}{24}\right) \tag{3d}$$

In this formulation, current propagation time is expressed with (t_y, t_m, t_d, t_h), corresponding to the year, month, day, and hour (e.g., terrestrial time) of the current simulation epoch.[8] Thus, when a torus-intersection is detected with Eq. (1), the instantaneous longitude of intersection is determined with Eq. (2), and the total CPE count for the appropriate torus cell is updated. Again, note that because of the convenient invariance of this torus geometry, the inertial RSO coordinates obtained during numerical integration do not need to be converted into the rotating Earth-centered, Earth-fixed reference frame to check for intersections. This elegant property provides for significant computational speedups that enable shorter simulation runtimes.

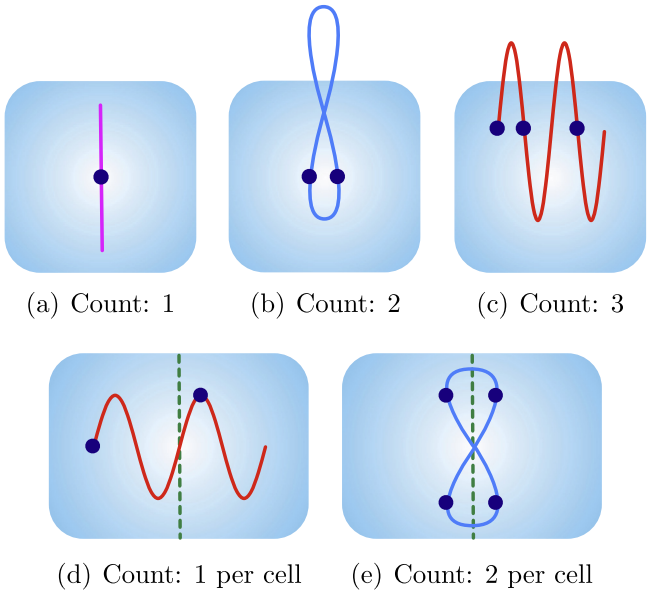

Fig. 5. Examples of counting logic that eliminates redundancy in intersection checking.

To ensure that similar intersection events are not accounted for more than once during CPE checking, counting logic is employed *before* a cell intersection counter is updated to "screen" the event for redundancy. Fig. 5 illustrates several examples as to how near-miss intersection events are counted during simulations. Relative orbits that reside entirely within a particular torus cell, as depicted in Fig. 5(a), are counted only once during the specified CPE tracking interval[9]; if the RSO exits and subsequently re-enters this torus cell, however, additional near-miss events are accounted for following each re-entry, as shown in Fig. 5 (b) and (c). Furthermore, additional near-miss events are counted if the relative orbit drifts into a neighboring cell during the CPE tracking interval of interest; Fig. 5(d) and (e) illustrate situations in which one and two near-misses are recorded per cell, respectively. This counting methodology ensures that near-miss events are tracked for each of the longitude slots in a logical, consistent, and non-redundant manner for the entirety of the interval. After propagating through the full interval, all cell counts are output and zeroed, and propagation continues.

[8] For concise explanation as to the Julian date and time parameters used in this method, the reader is referred to Curtis (2005).

[9] Arbitrary CPE tracking intervals are predefined to catalog intersections in consistent, reoccurring time frames. For this study, near-miss events are tracked in one-day intervals; after every day of propagation, torus cell counts are output to data files and then zeroed.

The complete algorithm for determining near-miss events with the torus scheme is detailed in A.

3.3. Propagator and implementation

During propagation of the trackable GEO debris population, eighth-order Gauss–Jackson methodology (Berry and Healy, 2004) is used to numerically integrate the equations of motion under a force model representative of the geosynchronous regime. Here, an 8×8 spherical harmonics expansion of the Earth's gravitational field is implemented with third-body luni-solar perturbations and nominal solar radiation pressure (SRP). Specifically,

$$\ddot{\boldsymbol{r}} = -\frac{\mu_\oplus}{r^3}\boldsymbol{r} + \boldsymbol{a}_\oplus + \boldsymbol{a}_\leftmoon + \boldsymbol{a}_\odot + \boldsymbol{a}_{\mathrm{SRP}} \tag{4}$$

where the first term denotes Keplerian two-body acceleration, $\boldsymbol{a}_\oplus$ is the acceleration due to the nonsphericity of Earth, $\boldsymbol{a}_\leftmoon$ and $\boldsymbol{a}_\odot$ are the third-body contributions from the Moon and Sun, respectively, and $\boldsymbol{a}_{\mathrm{SRP}}$ is the solar radiation pressure acceleration. Specifically, $\mu_\oplus \equiv GM_\oplus$ is the gravitational parameter of the Earth, and $r \equiv \|\boldsymbol{r}\|$ is the magnitude of the inertial position vector. In the non-inertial Earth-centered, Earth-fixed frame (i.e., ITRF-93), $\boldsymbol{a}_\oplus$ is written (Vallado, 2007)

$$a_\oplus^x = \left(\frac{1}{r}\frac{\partial U}{\partial r} - \frac{r_z}{r^2\sqrt{r_x^2+r_y^2}}\frac{\partial U}{\partial \phi}\right) r_x - \left(\frac{1}{r_x^2+r_y^2}\frac{\partial U}{\partial \lambda}\right) r_y \tag{5}$$

$$a_\oplus^y = \left(\frac{1}{r}\frac{\partial U}{\partial r} - \frac{r_z}{r^2\sqrt{r_x^2+r_y^2}}\frac{\partial U}{\partial \phi}\right) r_y + \left(\frac{1}{r_x^2+r_y^2}\frac{\partial U}{\partial \lambda}\right) r_x \tag{6}$$

$$a_\oplus^z = \frac{r_z}{r}\frac{\partial U}{\partial r} + \frac{\sqrt{r_x^2+r_y^2}}{r^2}\frac{\partial U}{\partial \phi} \tag{7}$$

where $\boldsymbol{r} \equiv (r_x, r_y, r_z)^T$ is the RSO position vector expressed within the Earth-centered, Earth-fixed reference frame, ϕ and λ denote geocentric latitude and longitude, respectively, and the partial derivatives are written (Vallado, 2007)

$$\frac{\partial U}{\partial r} = -\frac{\mu_\oplus}{r^2}\sum_{l=2}^{\infty}\sum_{m=0}^{l}\left(\frac{R_\oplus}{r}\right)^l (l+1)P_{l,m}(\sin\phi) \times [C_{l,m}\cos(m\lambda) + S_{l,m}\sin(m\lambda)] \tag{8}$$

$$\frac{\partial U}{\partial \phi} = \frac{\mu_\oplus}{r}\sum_{l=2}^{\infty}\sum_{m=0}^{l}\left(\frac{R_\oplus}{r}\right)^l \times [P_{l,m+1}(\sin\phi) - m\tan(\phi)P_{l,m}(\sin\phi)] \times [C_{l,m}\cos(m\lambda) + S_{l,m}\sin(m\lambda)] \tag{9}$$

$$\frac{\partial U}{\partial \lambda} = \frac{\mu_\oplus}{r}\sum_{l=2}^{\infty}\sum_{m=0}^{l}\left(\frac{R_\oplus}{r}\right)^l mP_{l,m}(\sin\phi) \times [S_{l,m}\cos(m\lambda) - C_{l,m}\sin(m\lambda)] \tag{10}$$

In this formulation, $R_\oplus = 6378.137$ km is Earth's equatorial radius, $P_{l,m}$ are the associated Legendre functions of degree l and order m, $C_{l,m}$ and $S_{l,m}$ are the un-normalized Stokes coefficients of the EGM-96[10] model, and

$$\sin\phi = \frac{r_z}{r} \tag{11}$$

$$\tan\lambda = \frac{r_y}{r_x} \tag{12}$$

Note that because Eqs. (5)–(7) are expressed within the rotating Earth-centered, Earth-fixed reference frame, this acceleration vector is transformed into inertial frame (i.e., J2000) coordinates during integration. The third-body accelerations arising from the direct and indirect effects of luni-solar gravitation are written (Vallado, 2007)

$$\boldsymbol{a}_\leftmoon = \mu_\leftmoon\left(\frac{\boldsymbol{r}_{j,\leftmoon}}{\|\boldsymbol{r}_{j,\leftmoon}\|^3} - \frac{\boldsymbol{r}_{\oplus,\leftmoon}}{\|\boldsymbol{r}_{\oplus,\leftmoon}\|^3}\right) \tag{13}$$

$$\boldsymbol{a}_\odot = \mu_\odot\left(\frac{\boldsymbol{r}_{j,\odot}}{\|\boldsymbol{r}_{j,\odot}\|^3} - \frac{\boldsymbol{r}_{\oplus,\odot}}{\|\boldsymbol{r}_{\oplus,\odot}\|^3}\right) \tag{14}$$

where $\boldsymbol{r}_{j,\leftmoon/\odot}$ is the inertial position vector from the jth RSO to the Moon/Sun, respectively, and $\boldsymbol{r}_{\oplus,\leftmoon/\odot}$ is the inertial position vector from the Earth to the Moon/Sun, respectively. The constants $\mu_\leftmoon \equiv GM_\leftmoon$ and $\mu_\odot \equiv GM_\odot$ denote the gravitational parameters for the Moon and Sun; thus, these third bodies directly influence GEO RSO orbits, and furthermore exert an indirect effect via gravitational interactions with Earth. The solar radiation pressure acceleration $\boldsymbol{a}_{\mathrm{SRP}}$ is modeled with the classical "cannonball" formulation (Vallado, 2007)

$$\boldsymbol{a}_{\mathrm{SRP}} = -p_{\mathrm{SRP}}c_r\beta\left(\frac{\boldsymbol{r}_{j,\odot}}{\|\boldsymbol{r}_{j,\odot}\|}\right) \tag{15}$$

where p_{SRP} is the solar radiation pressure at the altitude of the RSO orbit,[11] $c_r \equiv 1.5$ denotes the coefficient of reflectivity, and $\beta \equiv A_\odot/m$ is the area-to-mass ratio of the considered RSO. Schaub and Jasper (2011) indicate that $\beta \approx 0.04\ \mathrm{m^2/kg}$ is representative of the geostationary RSO population – this value is implemented for the "nominal" solar radiation pressure perturbation *for all* RSOs during propagation of the debris field, as specifying individual β_j for each RSO is a nontrivial matter and not in accordance with the purposes of this research.

The RSO propagation routine is written in ANSI-C and utilizes an eighth-order, predictor-corrector Gauss–Jackson integrator initialized with a Prince–Dormand 8(7) method (Berry and Healy, 2004; Jones and Anderson, 2012). Jones (2012) demonstrates the computational efficiency and accuracy of this integrator for near-circular geosynchronous orbits. During initial propagation of the debris field to the desired CPE start date, and during near-miss computations throughout the time frame of interest, the time step is specified as five minutes for

[10] Normalized Stokes coefficients for the EGM-96 gravity model are available from: <http://cddis.nasa.gov/926/egm96/egm96.html>

[11] Solar radiation pressure is modeled using the inverse-square diffusion formulation of solar luminosity $L_\odot \approx 3.839 \times 10^{26}$ J/s.

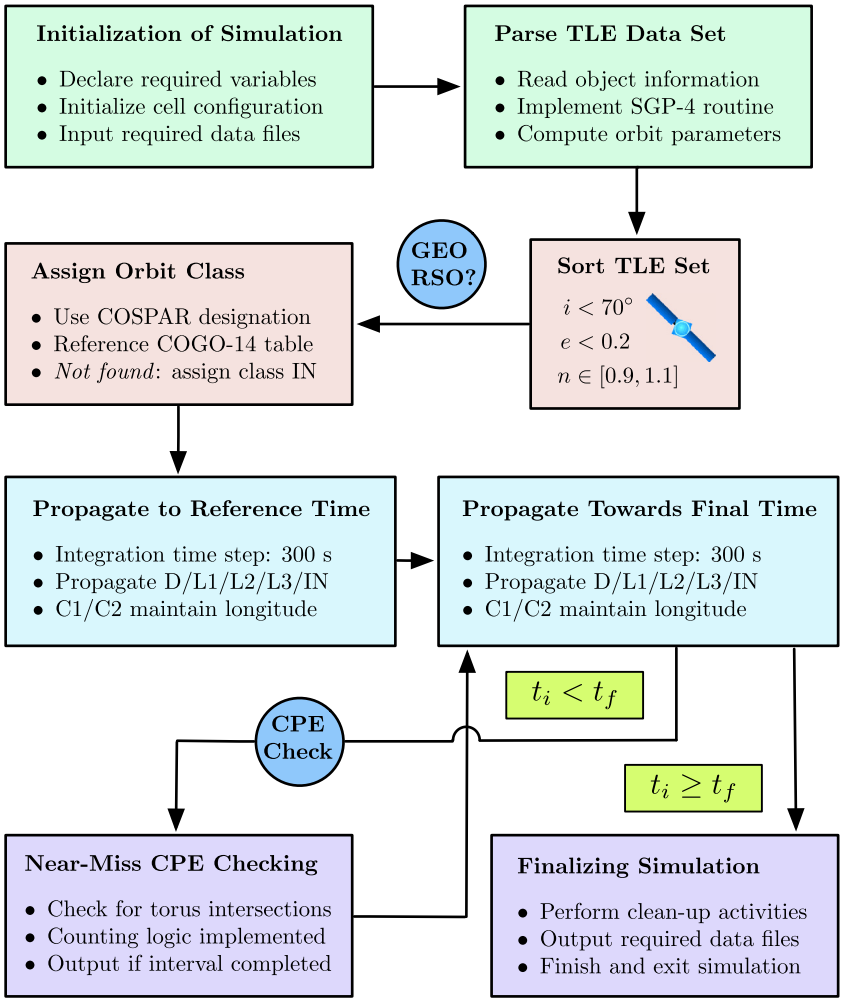

Fig. 6. High-level workflow for processing, propagation, and analysis of TLE data.

sufficient fidelity in CPE-checking activities.[12] Note that although this integrator and force model have been verified against NASA's General Mission Analysis Tool (GMAT)[13] for brief integration periods, they *are not intended* to offer a highly-accurate propagation utility.[14] A flowchart presenting a high-level description of GEO RSO processing, propagation, and analysis is provided in Fig. 6.

3.4. Results of debris flux study

The results of the geostationary debris flux analysis performed from March 2012–March 2013 for each of the four minor radius $\tilde{r}$ configurations considered are illustrated within Fig. 7. For this scenario, the GEO debris population was propagated without solar radiation pressure effects, and near-miss events were checked every five minutes of propagation with daily CPE intervals ($t_{\text{int}} = 86400$ s). Again, note that since this flux study only incorporates near-miss events for trackable, catalogued, and unclassified near-synchronous objects, these findings serve as a lower bound for the true debris flux situation in the GEO regime. As anticipated, as the torus radius $\tilde{r}$ increases, the near-miss CPE become more pronounced throughout the simulation space, exhibiting the severest debris weather at the locations of the Eastern ($\lambda = 75°$) and Western ($\lambda = 255°$) stable points for the entire one-year time frame. "Bunching" around the gravitational wells is a well-known result, as discussed in Chobotov (2002). Note that regions of increased near-miss events could be generated with (a) multiple RSOs with single events over the daily CPE

[12] Preliminary studies indicate that simulation results exhibit insignificant changes when smaller time step values, such as one minute, are employed. A five minute step is specified to decrease CPU time while still capturing the *macroscopic* trends sought by this research. Future work shall incorporate more extensive analysis to determine appropriate time steps for a given torus minor radius $\tilde{r}$, as would be required by higher-accuracy GEO flux studies.

[13] NASA's GMAT mission design software is open-source and publicly-available from: <http://gmat.gsfc.nasa.gov/>

[14] The purpose of this analysis is to highlight *macroscopic* patterns and trends in geosynchronous RSO motion. The propagation routine agrees with GMAT output to within 7-km RSS position discrepancy after one year of integration, suitable for the goals of this study.

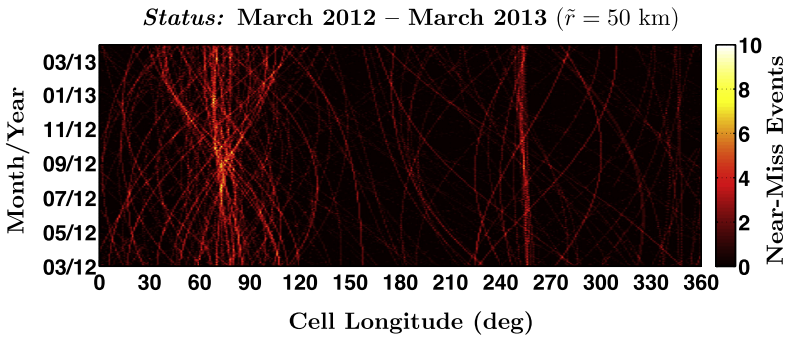

(a) Near-miss CPE for 03/12 – 03/13 for 50-km torus.

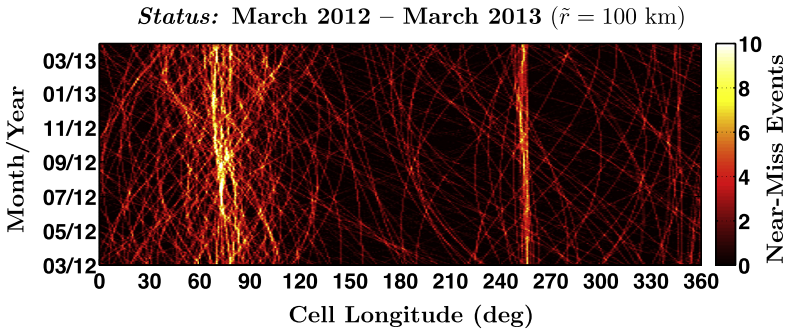

(b) Near-miss CPE for 03/12 – 03/13 for 100-km torus.

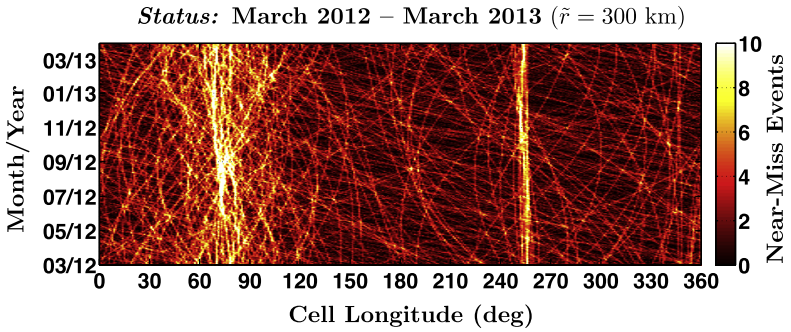

(c) Near-miss CPE for 03/12 – 03/13 for 300-km torus.

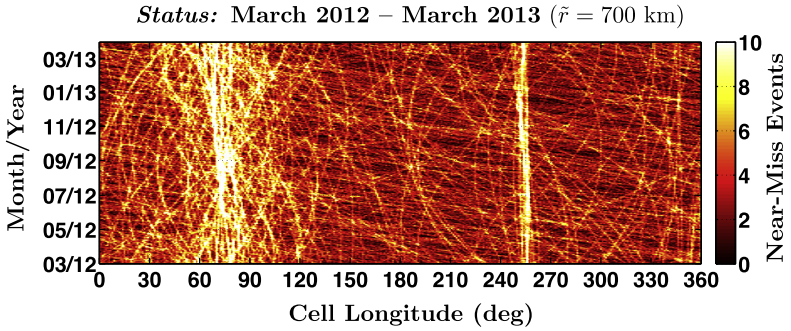

(d) Near-miss CPE for 03/12 – 03/13 for 700-km torus.

Fig. 7. Near-miss CPE for 03/12–03/13 without SRP.

interval, or (b) single RSOs with multiple intersection events over this CPE cycle, or (c) a combination of the above, in which complex relative motion induces the spatially-dense regions observed in Fig. 7.

The stochastic signature of the near-miss events illustrated within Fig. 7 emerges from a superposition of individual linear and quasi-linear traces generated by near-synchronous RSO orbits that deviate from the GEO

altitude; these objects demonstrate a drift magnitude indicated by the slopes of their observed traces. Traces of a positive slope indicate eastward precession (*below* GEO), while traces of negative slope conversely denote westward regression (*above* GEO). As all objects exhibiting mean motion $0.9 < n < 1.1$ revs/day are included in this analysis (Section 2.1), and noting that slopes of these traces are given with $(n - n_{\text{GEO}})^{-1}$, the observed slopes have an upper

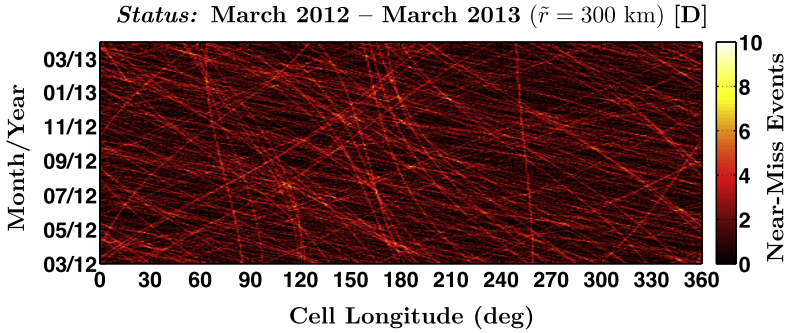

(a) Drifting object (D) contribution to near-miss CPE simulation.

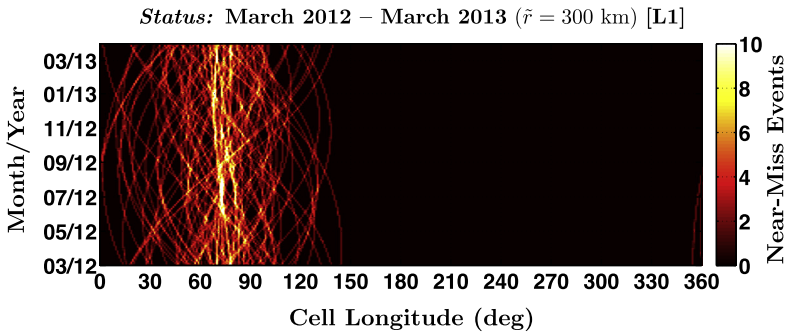

(b) Eastern librating object (L1) contribution to CPE simulation.

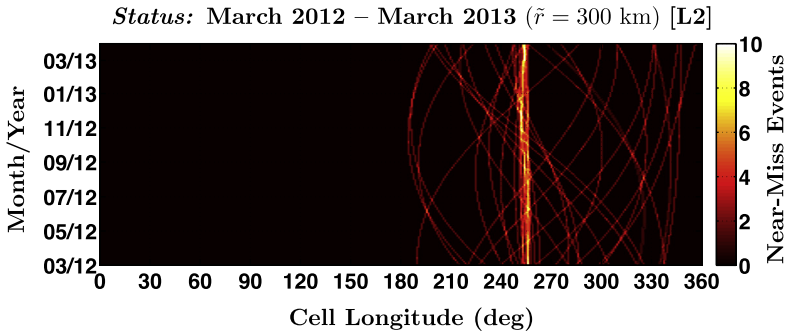

(c) Western librating object (L2) contribution to CPE simulation.

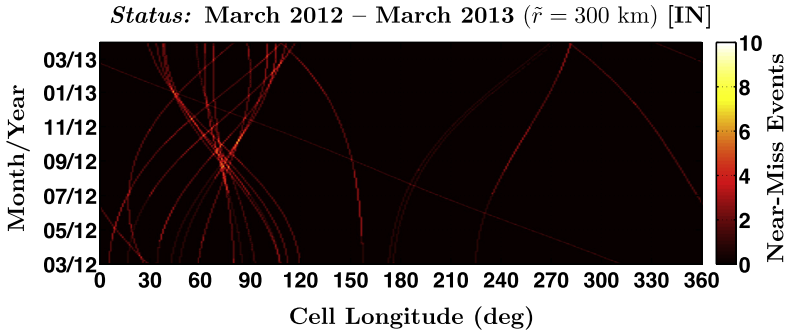

(d) Indeterminate object (IN) contribution to CPE simulation.

Fig. 8. Orbit class contributions to CPE for 300-km GEO torus.

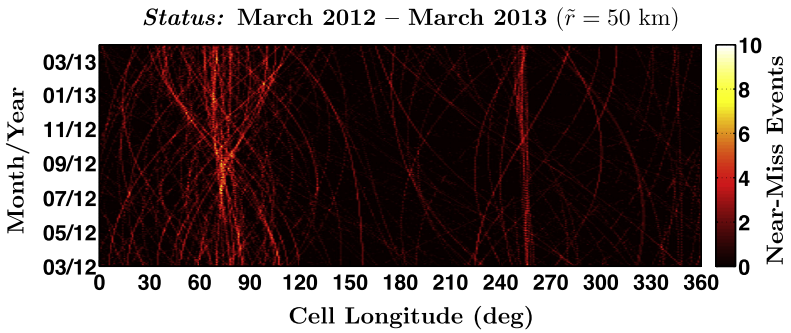

(a) Near-miss CPE for 03/12 – 03/13 for 50-km torus.

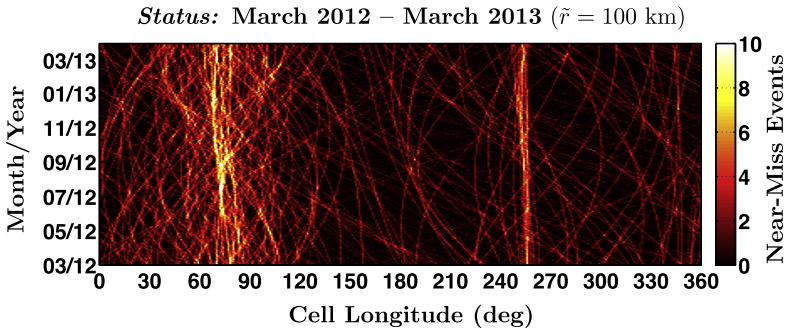

(b) Near-miss CPE for 03/12 – 03/13 for 100-km torus.

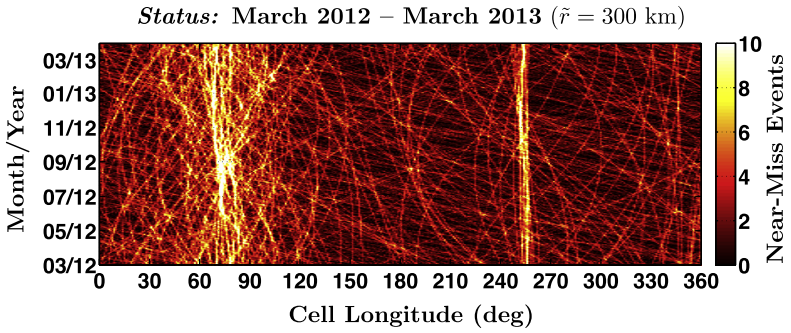

(c) Near-miss CPE for 03/12 – 03/13 for 300-km torus.

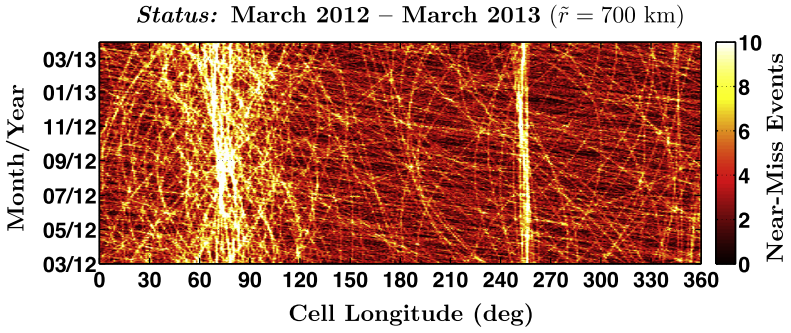

(d) Near-miss CPE for 03/12 – 03/13 for 700-km torus.

Fig. 9. Near-miss CPE for 03/12–03/13 with nominal SRP.

bound of 35°/day for the eastward-drifting RSOs, and −37°/day for the westward-drifting RSOs; objects exactly at GEO appear as vertical traces of an ∞ slope. Quasi-linear traces examined in Fig. 7 exhibit a curvature that arises from the oscillatory characteristic of the librating RSOs that reach their amplitude of oscillation and begin regressing, with a period of approximately 1.5 years at minimum (Allan, 1963).

Individual orbit class contributions to the $\tilde{r} = 300$ km case in Fig. 7(c) are depicted in Fig. 8. As D objects constitute half of the trackable RSO population at GEO (see Fig. 1), the drifting contribution is the most pronounced and visibly stochastic. Near-vertical traces of several RSOs drifting close to the GEO ring are perceptible in Fig. 8(a). Regions of increased RSO densities in the neighborhoods of the Eastern and Western stable points are driven primarily by near-miss contributions from the L1/L2 librating objects, as depicted within Fig. 8(b) and (c). The quasi-linear traces exhibited by the majority of IN objects in Fig. 8(d) indicate that these particular indeterminate RSOs may belong to one of the librating categories. Though the superposition of each of these class contributions yields a result that is of a more stochastic than deterministic signature, this macroscopic flux analysis illustrates the well-known result that regions of increased RSO congestion do exist locally, centered around the Eastern and Western stable points (Luu and Sabol, 1998; Chobotov, 2002). This localized congestion has important implications for satellite owners/operators with on-orbit assets in the neighborhoods of these "stormy" locations in the GEO ring.

With nominal solar radiation pressure included in the debris propagation, the results of an equivalent debris flux study performed from March 2012 to March 2013 for each of the four $\tilde{r}$ configurations are shown in Fig. 9. As anticipated, Fig. 9 illustrates no appreciable deviation from the case without nominal SRP displayed in Fig. 7. The area-to-mass ratio $\beta \approx 0.04$ m^2/kg used to simulate nominal SRP (Section 3.3) is not sizable enough to incur substantial differences in the simulation results in this one-year time frame. For lengthier CPE simulation time spans, it is critical to incorporate the long-term influence of SRP and the Earth's shadow, but for the purposes of this study, equivalent fidelity is achieved with or without this perturbation. The nominal, representative β value is low enough to ensure that the inclusion of SRP does not impact simulation findings.

4. Conclusion

An orbital debris flux study is performed in the geostationary ring to quantify the number of near-miss events occurring for each longitude slot at GEO. A geostationary torus configuration is implemented in tandem with publicly-available TLE data to simulate near-miss CPE incurred by the current GEO RSO population during the March 2012 to March 2013 time frame. Though the simulation results indicate that debris weather is primarily stochastic in nature, these findings confirm that two regions of increased RSO congestion exist at GEO, centered around the Eastern and Western stable points within the gravitational field. Although the frequency of near-miss events occurring at the GEO altitude is still relatively small as compared to LEO, appropriate remediation measures need to be implemented now, to protect the future usefulness of this natural resource and driver for space development, and preclude a situation similar to that now present within LEO.

Acknowledgements

The authors would like to acknowledge Brandon Jones and his TurboProp software (Hill et al., 2009), from which the ANSI-C integration routines employed in this research were obtained. The authors would also like to thank the reviewers of the original manuscript for providing insightful feedback.

Appendix A. Torus formulation CPE algorithm

Let t_i denote the epoch of the i^{th} RSO, and let t, t_{int}, and t_f denote the integration time, CPE interval time, and final simulation time, respectively. Define N_{RSO} as the number of geosynchronous RSOs, and $N_{\text{CPE}}|_{\lambda_{\text{bin}}}$ as the number of near-miss events for the torus cell indexed by longitude bin λ_{bin}. Furthermore, let $\mathcal{C}$ denote the set of all C1/C2 objects, and let $\mathcal{D}, \mathcal{L}$, and $\mathcal{I}$ be the sets of all D, L1/L2/L3, and IN objects, respectively. The algorithm for detecting near-miss events with the GEO torus formulation is as follows:

while $t_i < t_f$ **do**
  for $i = 1 \rightarrow N_{\text{RSO}}$ **do**
    Intersection flag $\leftarrow 0$
    Longitude flag $\leftarrow -1$
    if $i \in \mathcal{D} \cup \mathcal{L} \cup \mathcal{I}$ **then**
      while $t < t_{\text{int}}$ **do**
        Propagate: $t \leftarrow t + \Delta t \Rightarrow \boldsymbol{r}_{\text{RSO}} = (r_X, r_Y, r_Z)^T$
        if$(r_{\text{GEO}} - \sqrt{r_X^2 + r_Y^2})^2 + r_Z^2 - \tilde{r}^2 < 0$ **then**
        $t_h \leftarrow t_i + t/3600$
        Compute $\alpha_G \Leftarrow$ Eqs. (3a)–(3d)
        $\lambda_{\text{CPE}} = \texttt{atan2}(r_Y, r_X) - \alpha_G$
        $\lambda_{\text{bin}} = \text{floor}(\lambda_{\text{CPE}})$
        if Intersection flag $= 0$ || Longitude flag $\neq \lambda_{\text{bin}}$ **then**
          Increment: $N_{\text{CPE}}|_{\lambda_{\text{bin}}} \leftarrow N_{\text{CPE}}|_{\lambda_{\text{bin}}} + 1$
          Longitude flag $\leftarrow \lambda_{\text{bin}}$
        end if
      end if
      if $(r_{\text{GEO}} - \sqrt{r_X^2 + r_Y^2})^2 + r_Z^2 - \tilde{r}^2 < 0$
        Intersection flag $\leftarrow 1$
      else
        Intersection flag $\leftarrow 0$
      end if
    end while
    $t_i \leftarrow t_i + t_{\text{int}}$
    Update RSO fields
  else $(i \in \mathcal{C})$
    $t_i \leftarrow t_i + t_{\text{int}}$
    Update $\boldsymbol{r}_{\text{RSO}} \leftarrow \lambda_i$ maintained
    Update RSO fields
  end if
  end for
  Output $N_{\text{CPE}}|_{\lambda_{\text{bin}}} \forall \lambda_{\text{bin}} \in [0^\circ, 360^\circ)$
  $N_{\text{CPE}}|_{\lambda_{\text{bin}}} = 0 \forall \lambda_{\text{bin}} \in [0^\circ, 360^\circ)$
end while

References

Alfriend, K.T., Akella, M.R., Frisbee, J., Foster, J.L., Lee, D.-J., Wilkins, M. Probability of collision error analysis. Space Debris 1, 21–35, May, 1999.

Allan, R.R. Perturbations of a geostationary satellite by the longitude-dependent terms in the earth's gravitational field. Planet Space Sci. 11, 1325–1334. August, 1963.

Bendisch, J., Bunte, K., Klinkrad, H., Krag, H., Martin, C., Sdunnus, H., Walker, R., Wegener, P., Wiedemann, C. The master-2001 model. Adv. Space Res. 34, 959–968, 2004.

Berry, M.M., Healy, L.M. Implementation of Gauss–Jackson integration for orbit propagation. J. Astronaut. Sci. 52 (3), 331–357, 2004.

Chao, C.-C. Applied Orbit Perturbation and Maintenance. The Aerospace Press, 2005.

Chobotov, V.A. (Ed.). Orbital Mechanics, third ed., American Institute of Aeronautics and Astronautics, Inc, 2002.

Chrystal, P., McKnight, D., Meredith, P. Space debris: on collision course for insurers? Tech. rep., Swiss Reinsurance Company Ltd, 2011.

Curtis, H. Orbital Mechanics for Engineering Students. Elsevier Butterworth-Heinemann, 2005.

Flohrer, T. Classification of geosynchronous objects: Issue 14. Tech. Rep. 1, European Space Operations Centre, February 2012.

Hill, K., Jones, B.A. TurboProp Version 4.0. Colorado Center for Astrodynamics Research, University of Colorado at Boulder, May 2009.

Hoots, F.R., Roehrich, R.L. Spacetrack report no. 3: Models for propagation of norad element sets. Tech. rep., Office of Astrodynamics, Aerospace Defense Center, December 1980.

IADC/WG4, Iadc space debris mitigation guidelines. Tech. rep., IADC, September 2007.

Jehn, R., Agapov, V., Hernandez, C. The situation in the geostationary ring. Adv. Space Res. 35, 1318–1327, 2005.

Jehn, R., Hernandez, C. International practices to protect the geostationary ring. Space Debris 1, 221–233, 2001.

Johnson, N. Protecting the geo environment: policies and practices. Space Policy 15, 127–135, 1999.

Jones, B.A. Orbit propagation using Gauss–Legendre collocation, in: Proceedings of the 2012 AIAA/AAS Astrodynamics Specialist Conference, August 2012.

Jones, B.A., Anderson, R.L. A survey of symplectic and collocation integration methods for orbit propagation, in: Proceedings of the 22nd AAS/AIAA Space Flight Mechanics Meeting, February 2012.

Klinkrad, H. Space Debris: Models and Risk Analysis. Praxis Publishing, 2006.

Klinkrad, H., Alarcon, J.R., Sanchez, N. Collision avoidance for operational esa satellites, in: Proceedings of the Fourth European Conference on Space Debris, August 2005.

Lewis, H., Swinerd, G., Williams, N., Gittins, G. Damage: a dedicated geo debris model framework, in: Proceedings of the Third European Conference on Space Debris, vol. 1, ESA Publications Division, March 2001.

Liou, J.-C. An active debris removal parametric study for leo environmental remediation. Adv. Space Res. 47, 1865–1876, 2011.

Liou, J.-C., Hall, D.T., Krisko, P.H., Opiela, J.N. Legend: a three-dimensional leo-to-geo debris evolutionary model. Adv. Space Res. 34, 981–986, 2004.

Luu, K., Sabol, C. Effects of perturbations on space debris in supersynchronous storage orbits. Tech. rep., Air Force Research Laboratory, October 1998.

NASA. Process for limiting orbital debris. NASA-STD-8719.14 Change 4, National Aeronautics and Space Administration, September 2009.

Schaub, H., Jasper, L.E.Z. Circular orbit radius control using electrostatic actuation for 2-craft configurations, in: Proceedings of the 2011 AAS/AIAA Astrodynamics Specialist Conference, August 2011.

Vallado, D. Fundamentals of Astrodynamics and Applications, third ed Microcosm Press, 2007.

Vallado, D.A., Crawford, P., Hujsak, R., Kelso, T.S. Revisiting spacetrack report no. 3: Revision 2, in: Proceedings of the 2006 AIAA/AAS Astrodynamics Specialist Conference, August 2006.

Wegener, P., Bendisch, J., Krag, H., Oswald, M., Stabroth, S. Population evolution in the geo vicinity. Adv. Space Res. 34, 1171–1176, 2004.

Yasaka, T.. Space Debris: Hazard Evaluation and Mitigation. ESI Book Series. Taylor and Francis, Inc., pp. 113–131, 2002.

Yasaka, T., Hanada, T., Hirayama, H. Geo debris environment: a model to forecast the next 100 years. Adv. Space Res. 23 (1), 191–199, 1999.